Supporting Information for

Gaming Self-Consistent Field Theory: Generative Block Polymer Phase Discovery

Pengyu Chen and Kevin D. Dorfman

Kevin D. Dorfman
E-mail: dorfman@umn.edu

This PDF file includes:

Figs. S1 to S12
Table S1
Legends for Movies S1 to S3

Other supporting materials for this manuscript include the following:

Movies S1 to S3

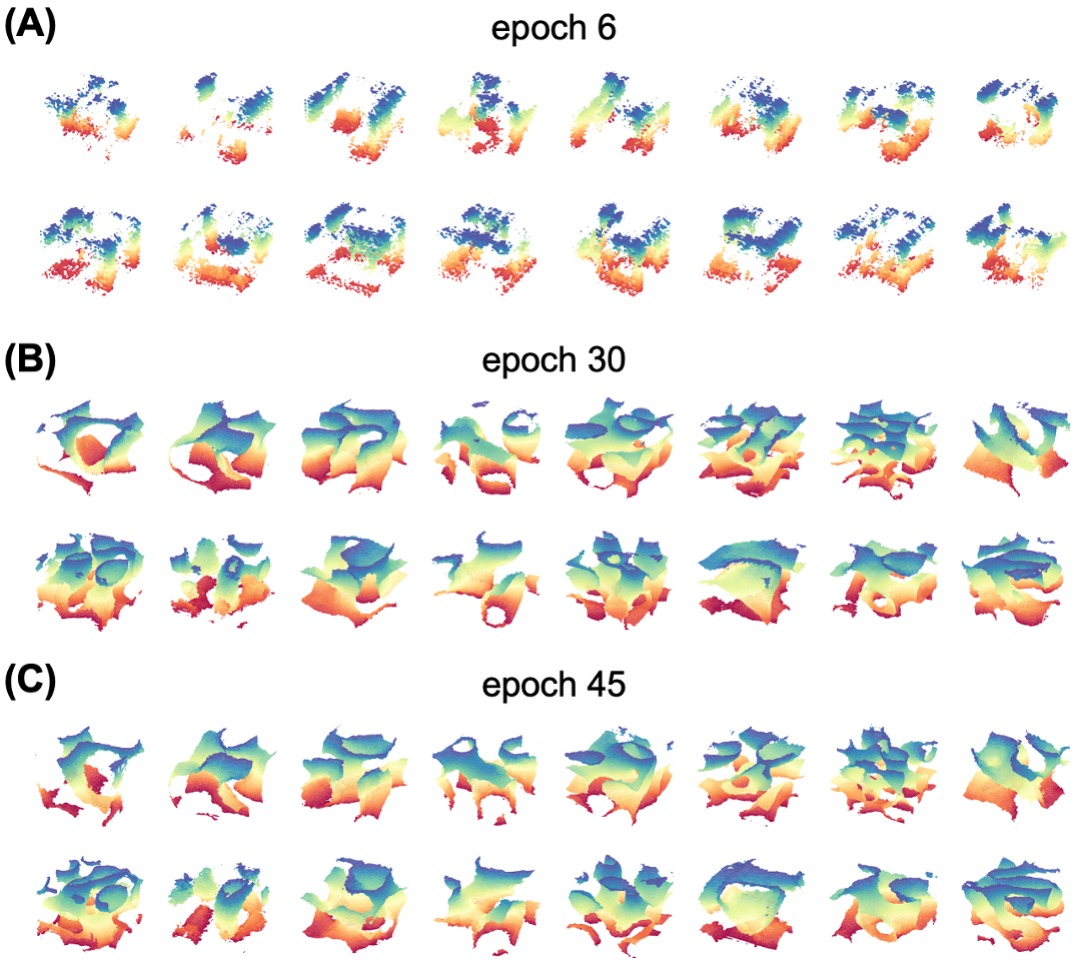

Fig. S1. 3D images generated by passing 16 fixed noises to the generator after training. (*A*) 6 epochs; (*B*) 30 epochs; and (*C*) 45 epochs. The colored surfaces are the isosurfaces with a value of 0.5. While the isosurfaces undergo considerable evolution between epochs 6 and 30, they show relatively little change between epochs 30 and 45.

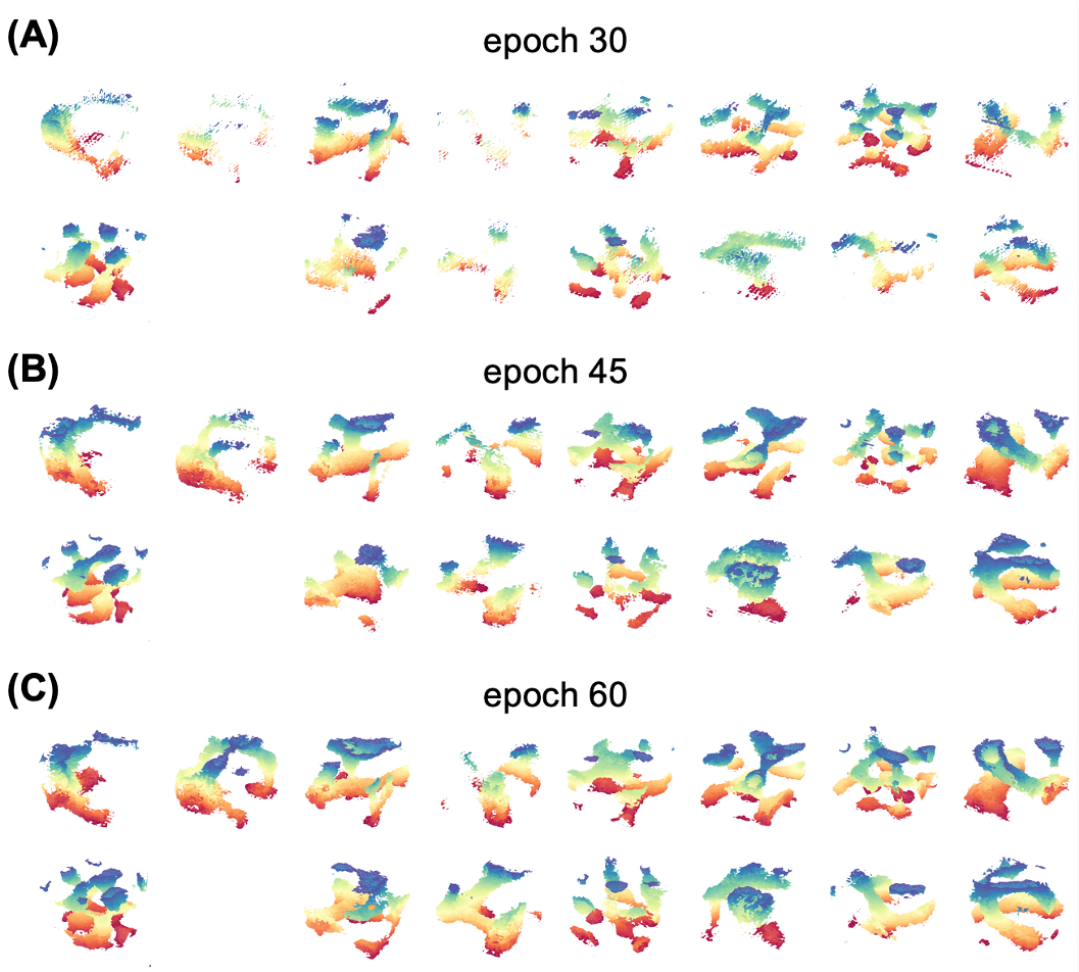

Fig. S2. 3D images generated by passing the same 16 fixed noises in Fig. S1 to the generator after training. (*A*) 30 epochs; (*B*) 45 epochs; and (*C*) 60 epochs. The colored surfaces are the isosurfaces with a value of 0.9. One of the images has a maximum value smaller than 0.9 during the training process. Although the isosurface plots with a value of 0.5 in Fig. S1 do not change much between epochs 30 and 45, there is a noticeable change for the isosurfaces with a value of 0.9. The change between epochs 45 and 60 is less pronounced, and thus the model after 45 epochs was chosen to generate initial guesses for SCFT calculations.

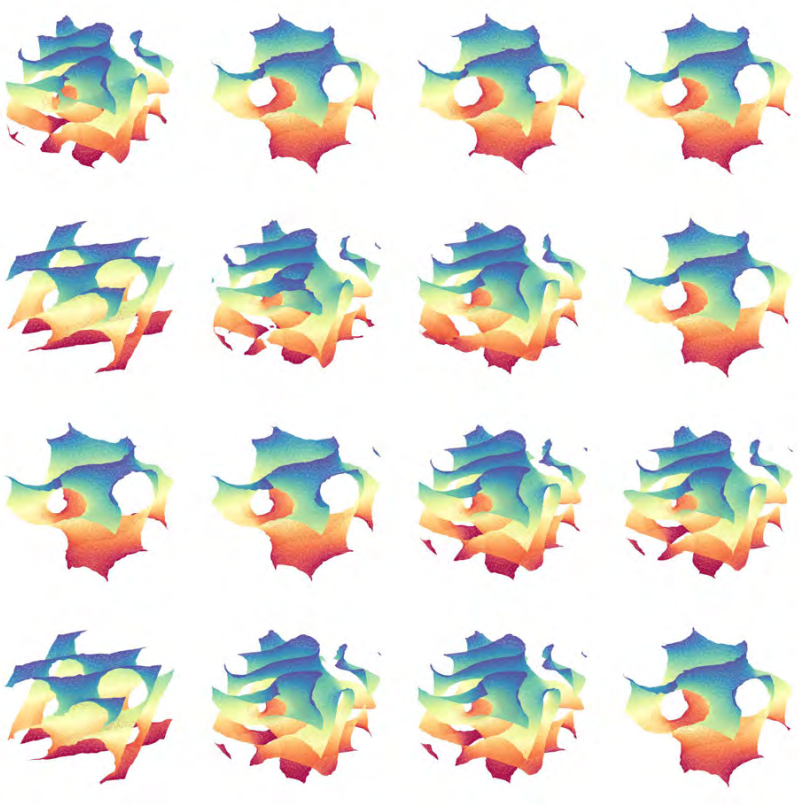

Fig. S3. Sixteen randomly generated density fields from GAN trained with SCFT trajectories of single gyroid, single diamond and double gyroid without data augmentation. The colored surfaces are the isosurface with a value of 0.5. With no random translations or rotations, the generated density fields exhibit similarities to the density field of a converged single gyroid, single diamond, or double gyroid solution, which are unlikely to produce any new candidate phase in SCFT.

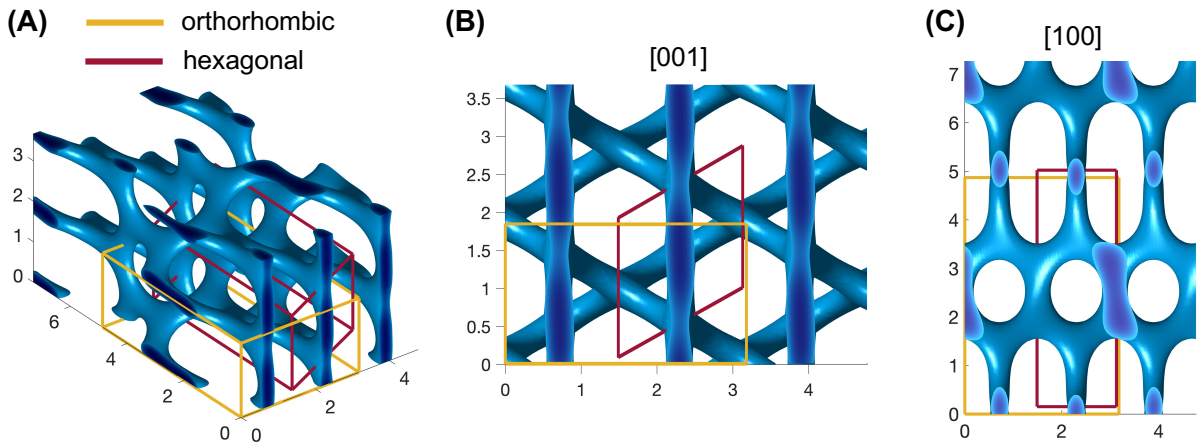

Fig. S4. Illustration of different unit-cell definitions of an identical structure using the example of H^{181}. Each panel (*A*), (*B*), and (*C*) provides a different projection of the H^{181} density profile with minority block density $\phi_{\mathrm{A}} > 0.9$. The length scale on the axes is in units of $R_e = \sqrt{N}b$, the unperturbed end-to-end distance of the polymer. The orthorhombic unit cell is the unit cell obtained from the SCFT solution using a GAN-generated initial guess, while the hexagonal unit cell is the conventional unit cell defined based on symmetry. Repeating either unit cell can produce the same H^{181} structures. Similar unit-cell conversions were applied to identify the conventional unit cells for the phases in Fig. 4*B*.

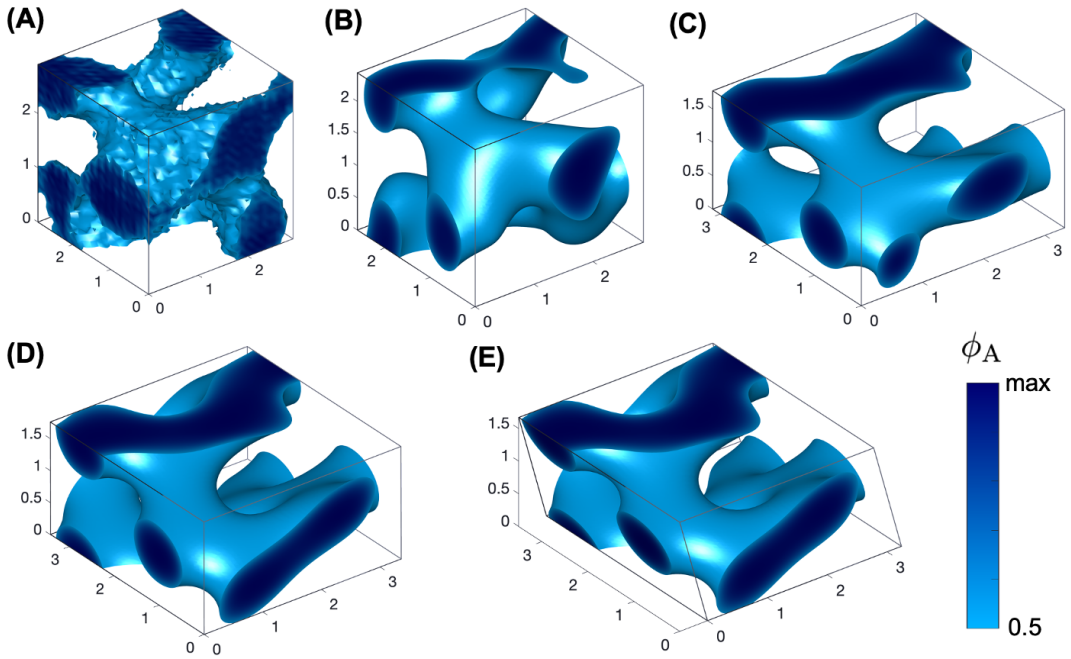

Fig. S5. Illustration of the convergence of a GAN-generated initial guess to the O^{70} phase in a flexible unit cell via SCFT. Minority block density distributions $\phi_{\mathrm{A}}(\boldsymbol{r})$ in a unit cell (*A*) for the GAN-generated initial guess; (*B*) after 21 SCFT iterations; (*C*) after 121 SCFT iterations; (*D*) after 259 SCFT iterations; and (*E*) for the converged solution (320 SCFT iterations). The 90-degree constraints on angles were removed after 259 iterations. The lengths on the axes are expressed in terms of the unperturbed end-to-end distance of the polymer, $R_e = \sqrt{N}b$. The maximum value of the minority block density ϕ_{A} are (*A*) 0.988; (*B*) 0.999; (*C*) 0.983; (*D*) 0.964; and (*E*) 0.964.

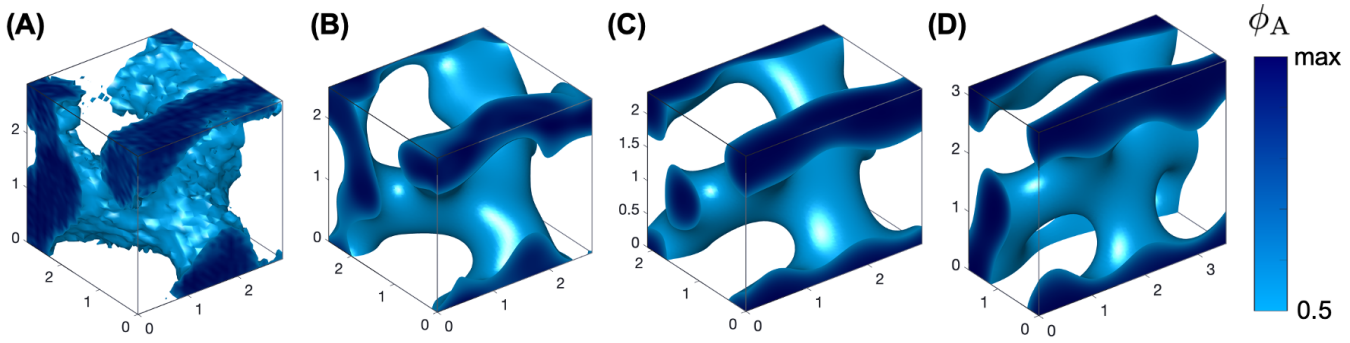

Fig. S6. Illustration of the convergence of a GAN-generated initial guess to the O^{52} phase in a flexible unit cell via SCFT. Minority block density distributions $\phi_{\mathrm{A}}(\boldsymbol{r})$ in a unit cell (*A*) for the GAN-generated initial guess; (*B*) after 11 SCFT iterations; (*C*) after 31 SCFT iterations; and (*D*) for the converged solution (197 SCFT iterations). The 90-degree constraints on angles were removed after 136 iterations, while the angles remained unchanged in the converged solution. The maximum value of the minority block density ϕ_{A} are (*A*) 0.988; (*B*) 0.982; (*C*) 0.977; and (*D*) 0.964.

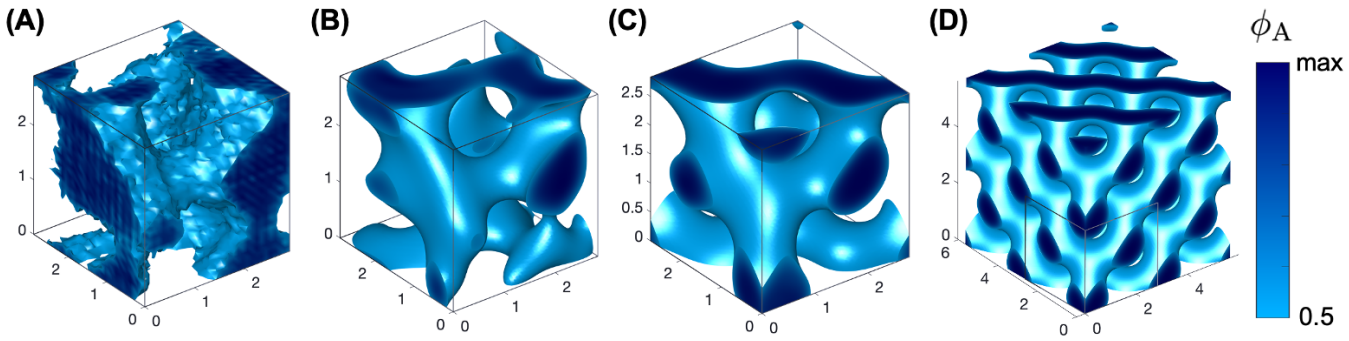

Fig. S7. Illustration of the convergence of a GAN-generated initial guess to the hexagonal perforated lamellae phase with ABC stacking (HPL) in a flexible unit cell via SCFT. Minority block density distributions $\phi_{\mathrm{A}}(\boldsymbol{r})$ in a unit cell (*A*) for the GAN-generated initial guess; (*B*) after 13 SCFT iterations; (*C*) after 41 SCFT iterations; and (*D*) for the converged solution (224 SCFT iterations). The 90-degree constraints on angles were removed after 93 iterations. The maximum value of the minority block density ϕ_{A} are (*A*) 0.993; (*B*) 1.014; (*C*) 0.985; and (*D*) 0.964.

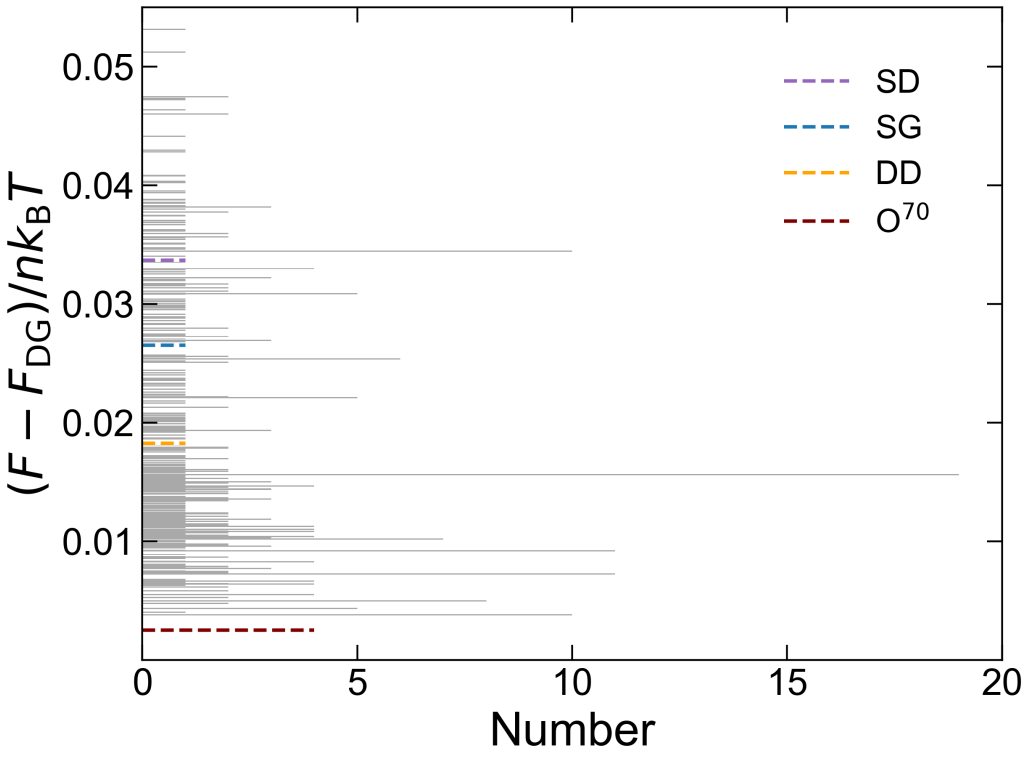

Fig. S8. Full histogram of the free energy per chain of the 349 metastable states produced by generative polymer field theory. A similar histogram for the metastable states with the lowest free energies is provided in Fig. 4*A*. A few known phases, including O^{70}, double diamond (DD), single gyroid (SG), and single diamond (SD), are labeled for reference. The free energies of the 349 metastable states span from 2.5×10^{-3} to 5.3×10^{-2} k_BT per chain above the equilibrium double-gyroid phase. 254 of these states have a lower free energy than single gyroid, and 198 of them have a lower free energy than double diamond. All of these metastable solutions have continuous networks or network-like perforated layers in the minority domain. The metastable phases with lower free energies typically contain either 3-fold connectors, 4-fold connectors, or both types of connectors. Network structures with 6-fold connectors were not found from the GAN-generated initial guesses, including the single-primitive and double-primitive phases, likely due to geometric packing frustration. The free energies of single and double primitive, obtained from SCFT converged solutions using previously converged solutions as the initial guess, are 6.3×10^{-2} and 9.9×10^{-2} k_BT per chain higher than the stable double-gyroid phase, respectively.

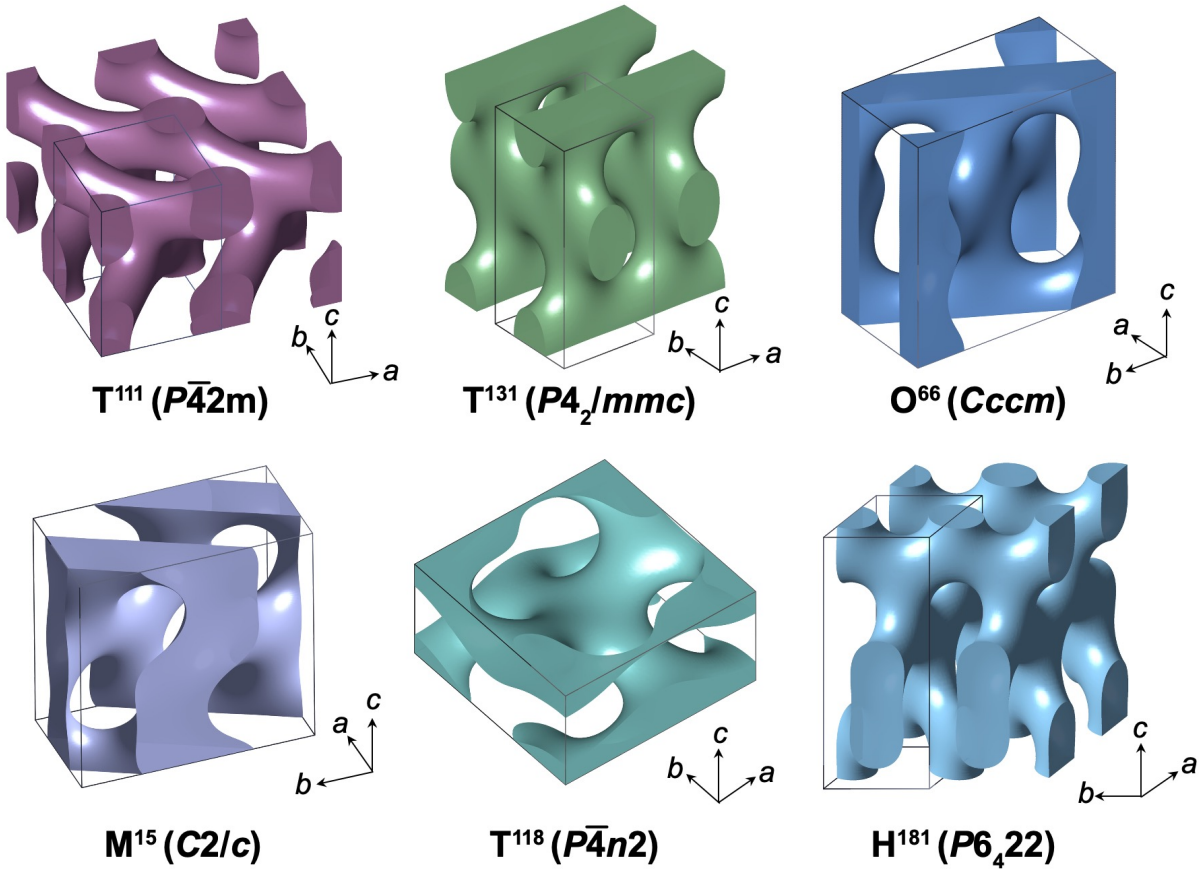

Fig. S9. Monomer density profiles for the candidate phases provided in Fig. 4*B*. The colored regions have minority block density $\phi_{\mathrm{A}} > 0.5$, and the boxes are the unit cell. The lattice parameters of these phases are: T^{111} ($[a, c] = [2.19, 3.00]$), T^{131} ($[a, c] = [1.59, 3.52]$), O^{66} ($[a, b, c] = [1.78, 3.34, 3.56]$), M^{15} ($[a, b, c, \beta] = [1.79, 3.48, 3.40, 90.0°]$), T^{118} ($[a, c] = [3.42, 1.73]$), and H^{181} ($[a, c] = [1.84, 4.87]$). The lengths in the unit cell parameters are normalized by the unperturbed end-to-end distance of the polymer, $R_e = \sqrt{N}b$.

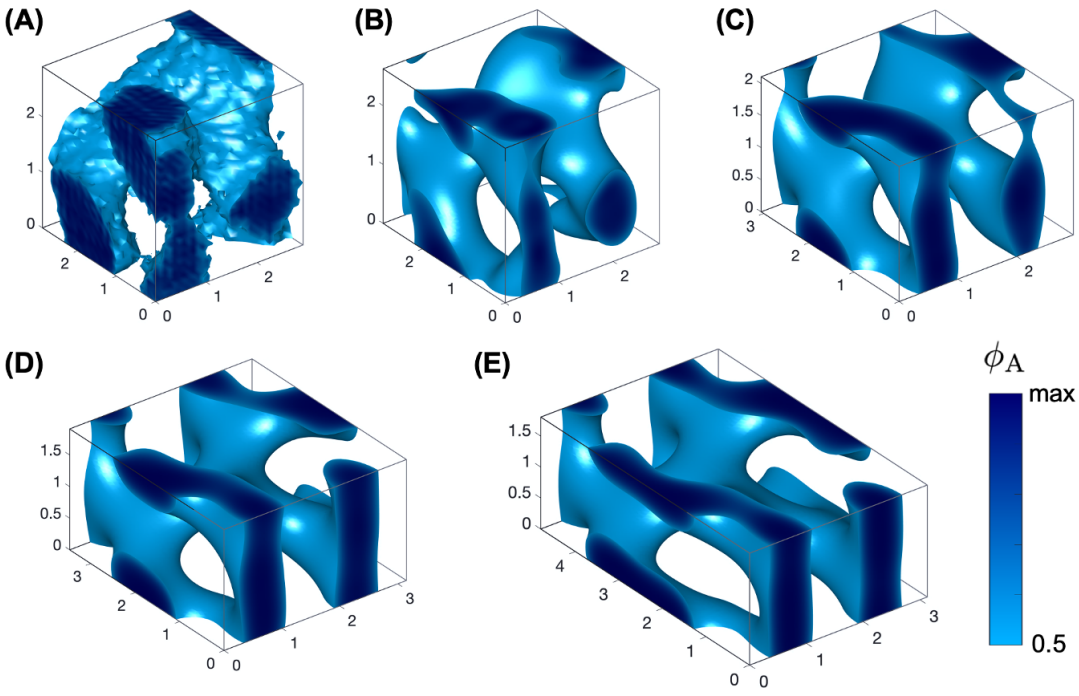

Fig. S10. Illustration of the convergence of a GAN-generated initial guess to the H^{181} phase in a flexible unit cell via SCFT. Minority block density distributions $\phi_{\mathrm{A}}(\boldsymbol{r})$ in a unit cell (*A*) for the GAN-generated initial guess; (*B*) after 11 SCFT iterations; (*C*) after 33 SCFT iterations; (*D*) after 65 SCFT iterations; and (*E*) for the converged solution (266 SCFT iterations). The 90-degree constraints on angles were removed after 143 iterations, while the angles remained unchanged in the converged solution. The maximum value of the minority block density ϕ_{A} are (*A*) 0.988; (*B*) 1.014; (*C*) 0.984; (*D*) 0.973; and (*E*) 0.964. A movie showing the complete SCFT trajectory is provided as Movie S3.

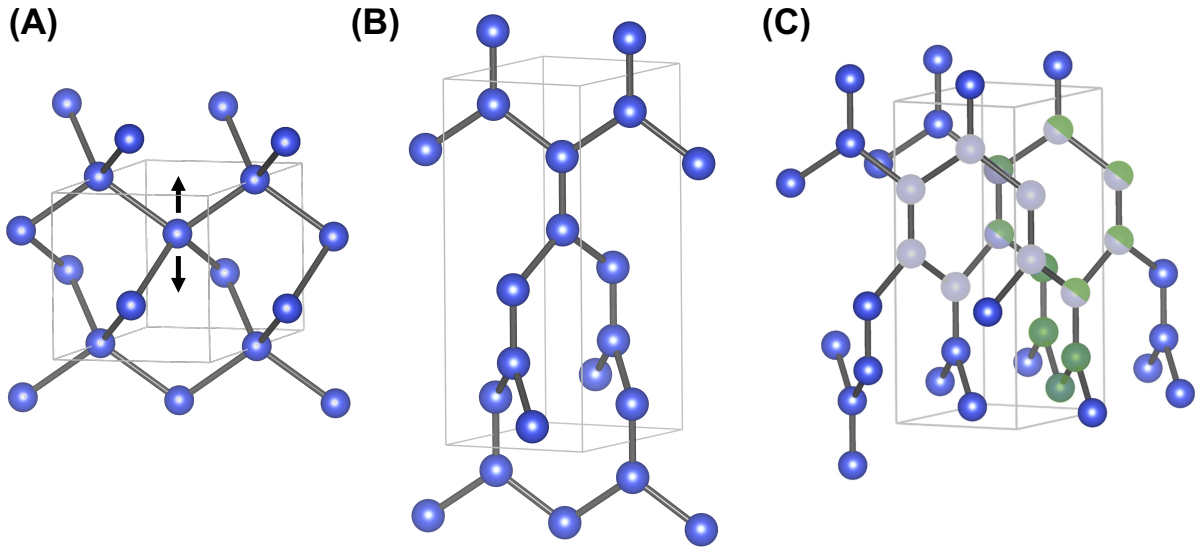

Fig. S11. Illustrations of the structural relationship between quartz network and the network of H^{181} candidate phase using ball-and-stick models to represent nodes and edges. (*A*) A model of the quartz network constructed by connecting the Si atoms of β-quartz with $P6_422$ symmetry. By splitting the 4-connected nodes along the c-axis into pairs of 3-connected nodes, (*B*) the network of the H^{181} phase can be obtained. (*C*) Illustration of 10-member rings (green) and 12-member rings (gray) in the H^{181} network.

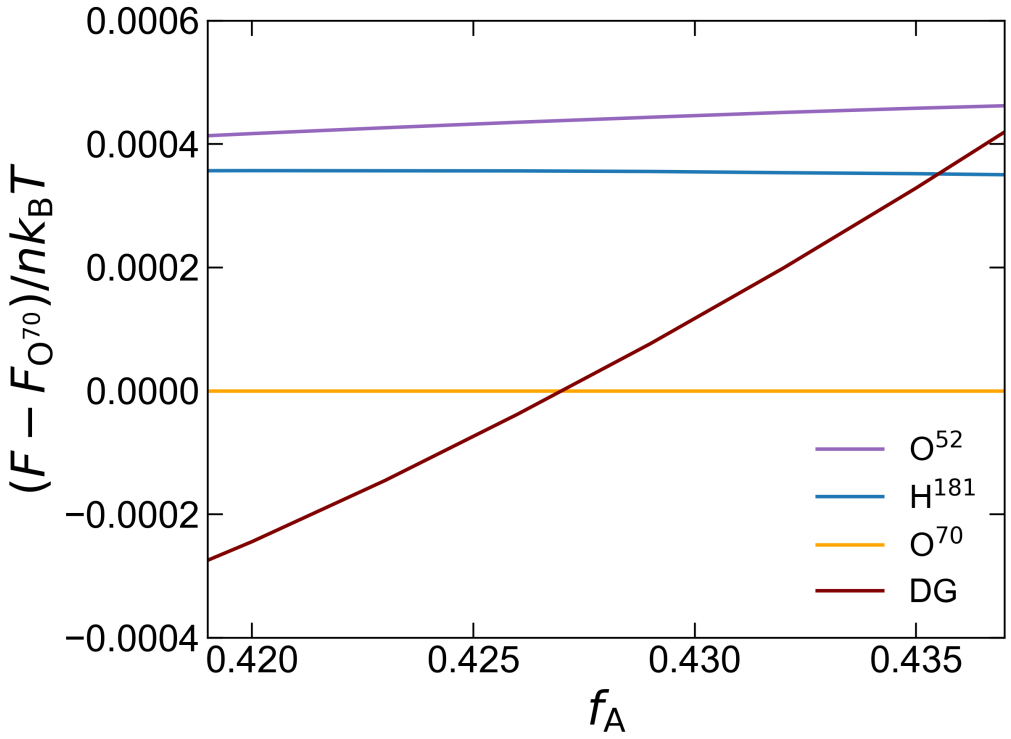

Fig. S12. Excess Helmholtz free energy per chain of the double gyroid (DG), O^{70}, H^{181} and O^{52} phases compared to O^{70} in the network stabilization region of the phase diagram of a conformationally symmetric linear diblock at $\chi N = 12$. The excess free energy of double gyroid compared to O^{70} increases as the block composition becomes more symmetric due to the differences in preferred curvatures, as illustrated in Fig. 5*D*. The excess free energy of H^{181} remains largely unchanged at different compositions, as indicated by the similarities in curvature distributions between the H^{181} and O^{52} phases.

Table S1. The GAN architecture used for generative polymer field theory with SCFT. Biases were incorporated in the 3D transposed convolutional layers (ConvTranspose3d) in the generator but were not included in 3D convolutional layers (Conv3d) in the discriminator. Zero-padding was used for padding operations. A negative slope of 0.2 was used for the Leaky ReLu (LReLu) activation function.

Layer	Operation	Output Dimensions	Kernel Size	Stride	Padding	Batch Norm	Activation
Generator input dimension: (100, 1, 1, 1)							
G_1	ConvTranspose3d	(512, 4, 4, 4)	(4, 4, 4)	1	0	Yes	ReLU
G_2	ConvTranspose3d	(256, 8, 8, 8)	(4, 4, 4)	2	1	Yes	ReLU
G_3	ConvTranspose3d	(128, 16, 16, 16)	(4, 4, 4)	2	1	Yes	ReLU
G_4	ConvTranspose3d	(1, 32, 32, 32)	(4, 4, 4)	2	1	No	Sigmoid
Discriminator input dimension: (1, 32, 32, 32)							
D_1	Conv3d	(64, 16, 16, 16)	(4, 4, 4)	2	1	Yes	LReLU
D_2	Conv3d	(128, 8, 8, 8)	(4, 4, 4)	2	1	Yes	LReLU
D_3	Conv3d	(256, 4, 4, 4)	(4, 4, 4)	2	1	Yes	LReLU
D_4	Conv3d	(1, 1, 1, 1)	(4, 4, 4)	1	0	No	Sigmoid

Movie S1. Evolution of the generated density fields during the training process of GAN.

Movie S2. The convergence of a GAN-generated initial guess to double-diamond phase via SCFT.

Movie S3. The convergence of a GAN-generated initial guess to H^{181} phase via SCFT.